焦子乐,李林,陈潇晶,等.改性风化煤铅修复剂的制备及其吸附机制[J].山西农业大学学报(自然科学版),2024,44(2):99-109.
Jiao Z L, Li L, Chen X J, et al.Preparation and adsorption mechanism of modified weathered coal lead remediating agent[J]. Journal of Shanxi Agricultural University(Natural Science Edition), 2024,44(2):99-109.
doi: 10.13842/j.cnki.issn1671-8151.202302027

改性风化煤铅修复剂的制备及其吸附机制

焦子乐[1,2],李林[1,2],陈潇晶[1,2,3],卢晋晶[1,2],郜春花[1,2],徐明岗[1,2],李建华[1,2*]

(1.山西农业大学 资源与环境学院,山西 太原 030031;2.土壤环境与养分资源山西省重点实验室,山西 太原 030031;
3.山西大学 黄土高原研究所,山西 太原 030006)

摘　要:[目的]风化煤来源广泛,价格低廉,且具有孔径分布合理、活性官能团丰富的特点,可通过改性提高其吸附性能,处理高浓度重金属废水,具有较大的开发价值。本文旨在以风化煤为原料制备一种高效的铅修复剂并对其吸附机制进行探究,以期为含铅废水的净化提供材料基础和理论支撑,同时为风化煤的高值化利用提供方向。[方法]采用乙烯胺改性、响应曲面法制备和优化风化煤修复剂的制备工艺,在批量吸附实验的基础上结合扫描电镜(SEM)、比表面及孔隙度分析仪(BET)、傅里叶变换红外光谱仪(FT-IR)、X射线衍射仪(XPS)等表征技术,对该材料的吸附机理进行探究。[结果]确定了三乙烯四胺改性风化煤制备铅修复剂的工艺参数:体系pH=4.98、乙烯胺用量2.58 mL·g^{-1}风化煤、超声时间为64.34 min、超声功率为350 W;该修复剂对铅的吸附过程符合拟二级动力学模型和Langmuir模型,表明该过程是以化学吸附为主的单分子层吸附,最大吸附容量达228 mg·g^{-1},较原煤提高了48%;热力学分析显示,$\Delta G<0$、$\Delta H>0$、$\Delta S>0$,即该反应是自发的吸热反应,且温度升高促进反应的发生;超声改性的破坏作用和三乙烯四胺的接枝使该修复剂的介孔面积减小了63.14%、微孔面积增大了126%,同时表面丰富的羟基、羧基、羰基、酰胺基等活性基团与铅发生配位或络合反应,促进了其对铅的捕获。[结论]本研究获得了一种高效的铅修复材料,乙烯胺用量和超声温度是影响该材料吸附性能的显著因素,微孔面积增大以及丰富的活性基团(羟基、羧基、羰基、酰胺基)是其主要的铅吸附机制。

关键词:风化煤; 乙烯胺改性; 铅污染; 响应曲面法
中图分类号:X172;X703　　**文献标识码**:A　　**文章编号**:1671-8151(2024)02-0099-11

随着原生铅冶炼、铅蓄电池、电镀、燃料、汽油、玻璃等工业的发展,大量的含铅废水被直接排放[1-2]。铅被列为第一类有毒污染元素,具有生物蓄积性强、毒性持久等特点[3-6],长期暴露在铅污染的场所中会造成人体的永久性损伤[7-8]。当人体内含有一定数量的铅时,血液和神经系统会被严重损害,尤其是对儿童的智力发育产生不可逆转的影响[9-10]。因此,铅污染废水问题亟待解决。

目前,铅污染废水常用的处理方法包括吸附、化学沉淀[11]、絮凝[12]、膜过滤[13]、离子交换[14]等,其中吸附法具有成本低、操作简单,无二次污染等优点,成为使用频率最高、适用范围最广的铅污染废水治理方法[1,15-16]。无机材料(沸石、生物质炭、硅藻土)[17-18]、有机材料(海藻酸钠、壳聚糖、琼脂)[19]以及有机无机复合材料等[20-21]是常见的吸附材料,但是利用煤基废弃资源作为重金属修复剂的研究鲜见报道。风化煤来源广泛价格低廉,且具有孔径分布合理、活性官能团丰富的特点,通过改性可提高其吸附性能[22],具有处理高浓度重金属废水的潜力,在解决环境污染问题的同时,实现风化煤的高效利用。作为一种低成本吸附剂,风化煤具有较大的开发价值。

本研究以风化煤为原料,三乙烯四胺(TETA)为改性剂,采用乙烯胺改性结合响应面

收稿日期:2023-02-22　　**修回日期**:2023-06-18
基金项目:国家重点研发项目(2020YFC1806504-03);山西省自然科学基金面上项目(202103021224137);山西省博士来晋奖励项目(SXBYKY2021089);山西农大博士科研启动项目(2021BQ48, 2021BQ49)
作者简介:焦子乐(ORCID:0000-0003-4225-8037),硕士研究生,研究方向:重金属修复剂的研发与应用。E-mail: jzl2573657313@163.com
*通信作者:李建华(ORCID:0009-0002-9305-9417),副研究员,博士,E-mail: jianhua0119@163.com

工艺优化法制备风化煤改性修复剂(JK-B)。在批量吸附实验的基础上结合扫描电镜(SEM)、比表面及孔隙度分析仪(BET)、傅里叶变换红外光谱仪(FT-IR)、X射线衍射仪(XPS)等表征技术,对该材料的吸附机理进行探究,以期为铅污染废水的修复提供材料基础和理论支撑,为风化煤的高值化利用提供方向。

1 材料和方法

1.1 试验材料

本实验使用的风化煤(JK)采自山西省交口县永兴煤矿,将其研磨、过筛(<75 μm)后作为载体原料。该风化煤的铅、铬、汞、镉、铜、镍、锌等重金属含量均低于相应的风险筛选值,腐殖酸含量大于30%(该风化煤的铅吸附容量为154 mg·g^{-1})。

1.2 试验方法

1.2.1 改性风化煤铅修复剂的制备方法

采用超声联合三乙烯四胺的方法改性风化煤。在5 g干燥风化煤中加入40 mL的去离子水,调节体系pH后加入一定体积的三乙烯四胺搅拌混匀并超声震荡,反复清洗固相至上清液呈中性,干燥后得改性风化煤铅修复剂JK-B[22]。

1.2.2 响应曲面法(Box-Behnken)优化制备工艺

响应曲面(Box-Behnken)设计用于优化超声改性工艺。以修复剂的铅吸附能力为依据,根据单因素预实验确定体系pH、乙烯胺用量、超声时间和超声功率的适当范围,以此确定响应曲面设计的因素水平(表1)。通过响应曲面法对结果进行分析,其变量按以下公式进行编码:

$$X_i=(x_i-x_0)/\Delta x_i(i=1,2,...k) \quad (1)$$

式中,X_i为自变量的编码值,x_i为自变量的真实值,x_0是自变量中心点的实际值,Δx_i是步长值。

以二次方程描述修复剂的铅吸附行为:

$$Y=\beta_0+\sum\beta_iX_i+\sum\beta_{ii}X_i^2+\sum\beta_{ij}X_iX_j(i,j=1,2,...k) \quad (2)$$

式中,Y为预测响应值(此处为单位铅吸附量或去除率),β_0为偏移项,β_i为线性效应,β_{ii}为平方效应,β_{ij}为交互效应,X_i和X_j为自变量的编码值。

1.2.3 批量吸附实验

用铅粉和硝酸配置1000 mg·L^{-1}的硝酸铅储备液(参照国标HJ 491-2019),稀释至所需浓度模拟含铅废水。

表1 响应曲面因素水平表

Table 1 Response surface factor level table

因素 Factors		水平对应值 Horizontal corresponding value		
		-1	0	1
体系pH	X_1	4	5	6
乙烯胺用量/mL	X_2	2.0	2.5	3.0
超声时间/min	X_3	40	60	80
超声功率/W	X_4	300	350	400

称取定量的修复剂置于50 mL硝酸铅溶液中,在恒温摇床((28±1)℃、180 r·min^{-1})中进行吸附实验。吸附完成后以4000 r·min^{-1}离心10 min,取上清液过0.45 μm滤膜,测定液相中铅浓度(AAS,240/240FS,Agilent,美国)。所有试验均设置3次平行,以未添加吸附剂为空白对照,排除铅的自发沉淀与损失。该修复剂在不同吸附条件下对铅的吸附量和吸附率根据(3)和(4)计算[23]:

$$q_e=\frac{(C_0-C_e)V}{W} \quad (3)$$

$$\eta=\frac{C_0-C_e}{C_0}\times 100\% \quad (4)$$

式中,q_e为吸附平衡时的吸附量(mg·g^{-1}),C_0为溶液初始浓度(mg·L^{-1}),C_e为吸附平衡液相浓度(mg·L^{-1}),V为溶液体积(L),W为吸附剂质量(g)。

1.2.4 吸附动力学和吸附热力学

使用拟一级、拟二级和颗粒内扩散3个吸附动力学模型来拟合动力学试验结果。

$$q_t=q_e(1-e^{-k_1t}) \quad (5)$$

$$\frac{t}{q_t}=\frac{t}{q_e}+\frac{1}{k_2q_e^2} \quad (6)$$

$$q_t=k_3t^{0.5}+C \quad (7)$$

式中,q_t和q_e分别为修复剂在平衡时刻和t时刻的

铅吸附量(mg·g^{-1});k_1(h^{-1})、k_2(mg·g^{-1}·h^{-1})、k_3(mg·g^{-1}·h$^{-1/2}$)依次为3种动力学模型的吸附常数;C为边界层厚度的常数(mg·g^{-1})。

使用Langmuir和Freundlich的2个等温模型来拟合等温吸附数据。

$$q_e = q_m \frac{k_L C_e}{1 + k_L C_e} \tag{8}$$

$$q_e = k_F C_e^{1/n} \tag{9}$$

其中,q_m为修复剂的理论最大铅吸附量(mg·g^{-1});k_L和k_F分别2个等温模型的常数;C_e为溶液铅离子的平衡浓度(g·L^{-1});n为指数因子,表示吸附强度。此外用R_L来描述吸附特性:

$$R_L = \frac{1}{1 + k_L C_0} \tag{10}$$

其中C_0是初始铅浓度(mg·L^{-1}),$0<R_L<1$时有利于吸附,$R_L>1$时不利于吸附,$R_L=0$时吸附是不可逆的。

利用平衡吸附常数K_L计算热力学参数,公式如下:

$$\Delta G = -RT\ln K_c \tag{11}$$

$$K_C = 10^6 \times K_L \tag{12}$$

$$\ln K_C = \frac{-\Delta H}{RT} + \frac{\Delta S}{R} \tag{13}$$

式中,R为气体常数(8.314 J·mol^{-1}·K^{-1}),T(K)为热力学绝对温度,K_C为标准吸附常数,可由公式(11)换算得到;ΔG可由式(9)直接计算,ΔH(KJ·mol^{-1})和ΔS(KJ·mol^{-1}·K^{-1})可由ln$K$与1/T关系图中的斜率和截距得出。

1.2.5　结构表征

采用场发射扫描电镜(SEM,MIRA4,泰思肯,捷克)和能谱色散仪(EDS,Xplore,泰思肯,捷克)对材料表面的形貌和微观结构及元素组成进行观察;采用傅里叶变换红外光谱仪(FTIR,Nicolet iS20,Thermo Fisher,美国)和X射线电子能谱仪(XPS, K-Alpha,Thermo Fisher S 1Ecientific,美国)对材料表面的官能团进行分析。

1.3　数据处理

运用Design-Export 12进行响应曲面实验设计,以材料的单位铅吸附量和去除率为响应值进行模型拟合和方差分析,使用Origin 2021进行图像绘制。

2　结果与讨论

2.1　修复剂的制备

2.1.1　响应面优化改性工艺

按表1列出的因素水平进行响应面设计,研究改性条件对修复剂的铅吸附容量、吸附率的影响,优化乙烯胺改性风化煤的制备工艺,响应面设计及结果如表2所示。通过回归分析得到二阶多项式方程如式(14)和(15),其中,Y_1和Y_2为修复剂的单位铅吸附量(mg·g^{-1})和去除率(%),X_1、X_2、X_3和X_4分别为体系pH、乙烯胺用量、超声时间和超声功率的实际值。

$$Y_1 = -1\,358.39 + 172.04X_1 + 301.31X_2 + 4.96X_3 - 7.72X_1X_2 - 0.07X_1X_3 + 0.01X_1X_4 + 0.44X_2X_3 + 0.07X_2X_4 - 0.002X_3X_4 - 15.24X_1^2 - 61.01X_2^2 - 0.04X_3^2 - 0.005X_4^2 \tag{14}$$

$$Y_1 = -3.274\,0 + 0.422\,6X_1 + 0.740X_2 + 0.012\,1X_3 - 0.007\,9X_1X_2 - 0.000\,2X_1X_3 + 0.001\,9X_2X_3 + 0.000\,2X_2X_4 - 0.038\,7X_1^2 - 0.151\,6X_2^2 - 0.000\,096X_3^2 - 0.000\,012X_4^2 \tag{15}$$

F检验(F-value)和概率P值(P-value)可检验回归方程各系数的统计意义,从而指示变量的相互作用[24]。由方差分析结果可知(表3),模型Y_1和Y_2的F-value分别35.09和33.22,P值均小于0.000 1,失拟项P(P_1=0.21,P_2=0.28)均大于0.05,表明模型拟合非常显著且失拟项不足,可用于描述因子与响应值之间的关系。线性项目(X_2、X_3)、二次项(X_1^2、X_2^2、X_3^2、X_4^2)和相互作用项(X_1X_2、X_2X_3)的系数对于Y_1和Y_2是显著的($P<0.05$),即乙烯胺用量、超声温度、体系pH与乙烯胺用量的交互作用,乙烯胺用量和超声温度的交互作用,以及各因子的二次项均与修复剂的单位铅吸附量和

表2 修复剂改性工艺优化的响应面设计及结果

Table 2 Response surface design and results of the optimization of modified remediation agent production process

编号 Number	变量水平 Variable Level[a]				吸附容量 Adsorption capacity	吸附率 Adsorption rate
	X_1	X_2	X_3	X_4	Y_1/(mg·g^{-1})	Y_2/%
1	4.00	2.00	60.00	350.00	159.66±1.41[b]	40.90±0.24
2	6.00	2.00	60.00	350.00	172.63±3.05	44.08±0.24
3	4.00	3.00	60.00	350.00	175.20±2.00	44.663±0.34
4	6.00	3.00	60.00	350.00	172.73±2.62	44.00±0.57
5	5.00	2.50	40.00	300.00	167.57±1.34	42.62±0.09
6	5.00	2.50	80.00	300.00	183.78±7.65	46.77±2.37
7	5.00	2.50	40.00	400.00	167.37±4.24	42.64±1.02
8	5.00	2.50	80.00	400.00	173.71±1.82	44.83±0.47
9	4.00	2.50	60.00	300.00	171.32±2.30	43.98±0.51
10	6.00	2.50	60.00	300.00	169.79±1.36	43.08±0.23
11	4.00	2.50	60.00	400.00	174.12±2.34	44.07±0.71
12	6.00	2.50	60.00	400.00	175.01±3.38	44.71±1.24
13	5.00	2.00	40.00	350.00	161.82±2.09	41.60±0.43
14	5.00	3.00	40.00	350.00	162.53±3.14	41.56±0.51
15	5.00	2.00	80.00	350.00	167.46±3.59	42.54±0.64
16	5.00	3.00	80.00	350.00	185.92±2.81	47.24±0.73
17	4.00	2.50	40.00	350.00	166.94±1.48	42.47±0.53
18	6.00	2.50	40.00	350.00	168.13±0.46	43.05±0.47
19	4.00	2.50	80.00	350.00	178.35±3.15	45.91±0.81
20	6.00	2.50	80.00	350.00	174.30±1.57	44.63±0.11
21	5.00	2.00	60.00	300.00	171.41±1.27	44.23±0.28
22	5.00	3.00	60.00	300.00	175.67±0.48	44.99±0.20
23	5.00	2.00	60.00	400.00	170.96±2.44	43.95±0.72
24	5.00	3.00	60.00	400.00	182.12±11.62	46.43±2.56
25	5.00	2.50	60.00	350.00	203.45±4.10	51.89±0.79
26	5.00	2.50	60.00	350.00	201.83±1.16	51.48±0.54
27	5.00	2.50	60.00	350.00	199.33±1.70	50.58±0.43
28	5.00	2.50	60.00	350.00	202.22±7.07	51.56±1.31
29	5.00	2.50	60.00	350.00	198.13±2.64	50.53±0.26

注:[a]采用Design-Expert 12进行试验设计,其中X_1代表体系pH,X_2乙烯胺用量,X_3超声时间,X_4固声功率;[b]标准差由3个独立样本计算得到

Note: Design-Expert 12 was adopted for experimental design; X_1: the pH of the system, X_2: the amount of ethylene amine, X_3: the ultrasonic time, X_4: the fixed sound power; b indicated that standard deviation was calculated from three independent samples

去除率显著相关。决定系数R_1^2=0.968 2,R_2^2=0.966 4,表明该模型具有较强的相关性[31],R_1^2-Adj. R_1^2=0.027 6<0.2,R_2^2-Adj. R_2^2=0.031 4<0.2,变异系数CV_1=1.74<10%,CV_2=1.76<10%,表明模型的可信度较高[32],Y_1和Y_2的信噪比分别为18.287 8和17.764 0,均大于4,表明以上模型是有效的[33]。综上所述,Y_1和Y_2能较好的拟合修复剂的铅吸附行为,能够用于修复剂制备工艺的优化。

2.1.2 响应面优化结果与验证

三维响应面图可以直观的反应被优化因素对响应值的影响。如图1所示,在响应面优化实验的基础上,根据2因素(X轴和Y轴)与响应值Z(Y_1和Y_2)绘制带投影的三维响应面图。图1显示体系pH与乙烯胺用量、乙烯胺用量与超声时间之间的响应面均是伞状的,且中心为位于设定范围内,这

表3　响应面方差分析(ANOVA)和回归方程

Table 3　Response surface analysis of variance (ANOVA) and credibility analysis of the regression equations

方差来源 Sources of variance	Y_1		Y_2	
	F—value	P—value	F—value	P—value
Model	35.09	<0.000 1	33.22	<0.000 1
X_1	0.432 1	0.520 9	0.323 1	0.578 2
X_2	22.16	0.000 3	17.52	0.000 8
X_3	42.02	<0.000 1	42.69	<0.000 1
X_4	0.124 9	0.728 7	0.109 1	0.745 7
X_1X_2	6.29	0.024 1	5.68	0.030 9
X_1X_3	0.720 6	0.409 3	1.37	0.259 6
X_2X_3	8.31	0.011 4	8.92	0.009 2
X_2X_4	1.25	0.280 9	1.19	0.293 1
X_3X_4	2.58	0.129 2	1.47	0.244 0
X_1^2	158.96	<0.000 1	154.49	<0.000 1
X_2^2	159.16	<0.000 1	148.28	<0.000 1
X_3^2	159.74	<0.000 1	151.09	<0.000 1
X_4^2	101.19	<0.000 1	94.19	<0.000 1
Lack of it	2.33	0.214 6	1.90	0.281 7

注:Y_1代表修复剂的铅吸附量,Y_2代表修复剂的铅去除率

Note: Y_1 represented the lead adsorption capacity of the restorative, Y_2 represented the lead removal rate of the restorative

表明修复剂的铅吸附性能较好,且该试验设计包括最优改性条件的水平[25]。

方差分析表明体系pH与乙烯胺用量之间的相互作用是显著的($P<0.05$)。如图1(A)、1(B)所示,吸附量和去除率响应面均较为陡峭,且对应等高线投影呈椭圆形,表明体系pH和乙烯胺用量之间的相互作用显著[24]。优化分析显示体系pH为4.98,乙烯胺用量为2.58 mL时,修复剂的单位铅吸附量和去除率接近响应面的最高值。如图1C、1D所示,吸附量和去除率的响应面弧度较大,且等高线投影呈椭圆形,表明乙烯胺用量和超声时间之间的相互作用显著。优化分析显示乙烯胺用量为2.58 mL,超声时间为64.34 min,改性效果最好。修复剂的单位铅吸附量和去除率分别达203.48 mg·g^{-1}和51.89%,较原煤提高了30.5%。

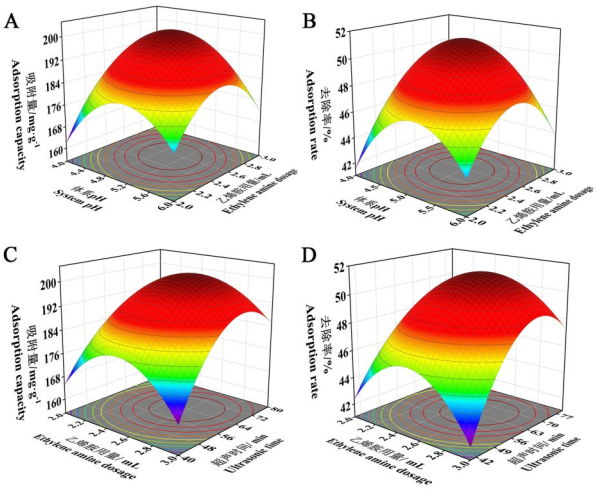

A为体系pH和乙烯胺用量对修复剂的单位铅吸附量响应曲面图;B为体系pH和乙烯胺用量对修复剂的铅去除率的响应曲面图;C为乙烯胺用量和超声时间对修复剂单位铅吸附量的响应曲面图;D为乙烯胺用量和超声时间对修复剂的铅去除率的响应曲面图

The response curve of the system pH and ethylene amine dosage to the unit lead adsorption capacity of repair agent (A); Response curve of system pH and ethylene amine dosage to lead removal rate of repair agent (B); The corresponding curve of the amount of ethylamine and the ultrasonic time on the adsorption amount of lead per unit of repair agent (C); Response surface of ethylene amine dosage and ultrasonic time to lead removal rate of repair agent (D)

图1　体系pH与乙烯胺用量、乙烯胺用量和超声时间的交互作用对修复剂吸附性能的影响

Fig.1　Effect of interaction between system pH and ethylene amine dosage, ethylene amine dosage and ultrasonic time on the adsorption performance of restorative

根据二次模型及响应面的分析,本研究实验范围内优化后的改性条件为:体系pH=4.98、乙烯胺用量2.58 mL·g^{-1}风化煤、超声时间64.34 min、超声功率为350 W。为了便于实际操作和分析,设定体系pH=5、乙烯胺用量为每克2.6 mL风化煤、超声时间为65 min、超声功率为350 W,该条件下的理论吸附容量为201.96 mg·g^{-1},去除率为51.5%。根据以上条件进行修复剂的制备,验证模型的预测精度,最终得到优化后的材料单位吸附容量199.70 mg·g^{-1},去除率为50.78%,预测精度高于95%。Ding等[29]将甘蔗渣改性后进行含铅

表4　回归方程的可行性分析

Table 4　Credibility analysis of the regression equations

指标 Index mark	标准差 Std. dev	平均值 Mean	变异系数/% CV	R^2	调整R^2 Adj. R^2	预测R^2 Pre. R^2	预测精准度 Ade precision
Y_1	3.08	177.02	1.74	0.968 2	0.940 6	0.849 8	18.287 8
Y_2	0.007 9	0.452 1	1.76	0.968 5	0.937 1	0.851 3	17.764 0

废水的吸附,其最大吸附容量为21 mg·g^{-1},Gao等[8]用麦草制备的生物炭最大吸附容量为157.95 mg·g^{-1},与国内外同类材料相比,本研究制备的修复剂处于较高的水平。据此获得1种吸附性能较好的改性风化煤修复剂。

2.2 修复剂结构表征

风化煤改性前后的扫面电镜图像分析如图2A和2B所示。改性后风化煤的表面更加破碎,颗粒整体变小且分布较为均匀。为了进一步了解该材料的孔隙特征,测定了改性前后的孔结构参数,改性后风化煤的N_2吸附体积低于改性前(图3A),并且比表面积由4.070 5 m^2·g^{-1}减至1.736 6 m^2·g^{-1},降低了57.33%,微孔面积由0.822 3 m^2·g^{-1}增至1.890 2 m^2·g^{-1},增加了126%,介孔面积由3.344 5 m^2·g^{-1}减至1.232 9 m^2·g^{-1},降低了63.14%(表4),这可能是超声改性破坏了风化煤中的部分介孔结构,同时三乙烯四胺中的多乙烯多氨基的附着和占位引起的[26]。

此外,对改性前后的风化煤进行了X射线衍射分析。由图3B可知,改性前风化煤表面主要由C1s和O1s元素组成,改性后在399.29 eV处出现N1s的特征吸收峰,表明改性后风化煤表面新增N元素。图3C、3D为改性前后风化煤表面的C1s谱图,根据魏金枝等[27]将C1s峰分为C—C/C=C,C—O,C=O共3个峰,改性后风化煤中C—C/C=C的相对含量从44.05%上升至65.24%,C—O的相对含量从43.28%下降至14.0%,C=O的相对含量从12.67%下降至11.47%,同时新增C—N,其相对含量为9.30%,这说明三乙烯四胺与风化煤是以C—N键形式相连,同时在反应过程中利用了部分C—O单键[26]。以上结果表明成功制备出了三乙烯四胺修饰的改性风化煤铅修复剂。

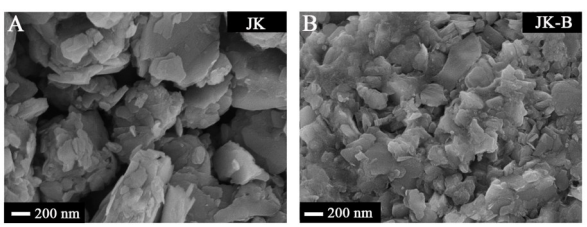

图2 改性前后的扫描电镜图像(A为改性前图像JK,B为改性后图像JK-B)

Fig.2 SEM images before and after modification (A is the image before modification JK, B is the image after modification JK-B)

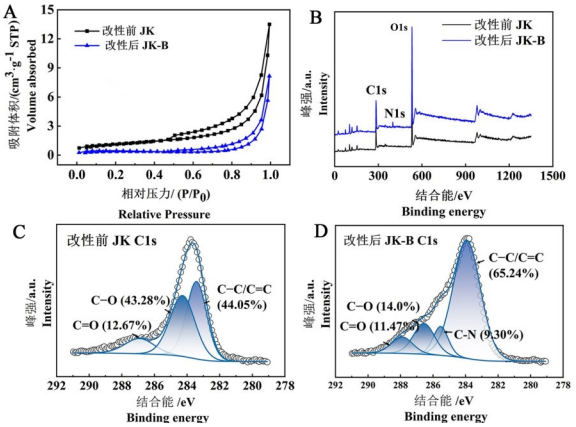

图3 改性前后的N_2吸脱附曲线(A)、X射线衍射谱图(B)及C1s分谱(C、D);JK代表改性前,JK-B代表改性后

Fig.3 N_2 adsorption-desorption curve (A), XPS spectrum (B), and C1s spectral before and after modification (C, D).JK represented before modification and JK-B represented after modification

表4 改性前后的孔结构参数

Table 4 Pore structure parameters before and after modification

样品 Sample	比表面积/(m^2·g^{-1}) S_{BET}	微孔/(m^2·g^{-1}) S_{mic}	介孔/(m^2·g^{-1}) S_{mes}	孔径/n D_{av}
JK	4.070 5	0.822 3	3.344 5	12.131 5
JK—B	1.736 6	1.890 2	1.232 9	12.151 5

2.3 修复剂铅吸附机制

2.3.1 吸附动力学分析

在铅浓度固定为200 mg·L^{-1}、材料用量为0.4 g·L^{-1}、溶液初始pH=4的条件下,研究了吸附时间对铅吸附的影响。采用拟一级、拟二级模型对实验数据进行拟合揭示修复剂的吸附特征,拟合模型及参数见图4A、表5。结果显示,该修复剂对铅的吸附容量可达209.39 mg·g^{-1},并且拟二级动力学模型的R^2高于拟一级动力学拟合结果,表明拟二级动力学模型可以更好地揭示铅在修复剂上的吸附,说明其对铅的吸附以化学吸附为主[28]。

为了进一步探索铅的吸附过程,采用颗粒内扩散模型对数据进行拟合。如图4B所示,修复剂的铅吸附容量与$t^{1/2}$在整个时间范围内可用2条不同斜率的直线拟合,且不通过原点,表明吸附过程均不受单一扩散因子的影响[28]。第1阶段为开始的1.5 h,约有203.20 mg·g^{-1}(占饱和吸附量的95.09%)铅被修复剂吸附,第2阶段发生在1.5 h

之后,约有5%的铅被吸附,并且到达吸附平衡。由表6中的颗粒内扩散参数可知,2阶段的斜率常数$K_{Ⅰ}>K_{Ⅱ}$。据此可将该修复剂对铅的吸附分为快慢2阶段,铅从溶液向修复剂表层迅速转移,占据大量吸附位点,随后较慢的相互作用归因于铅的颗粒内扩散,Ding[29]和Zhao等[28]采用生物炭、多孔有机材料等对溶液中铅的吸附研究也得到了类似的结果。

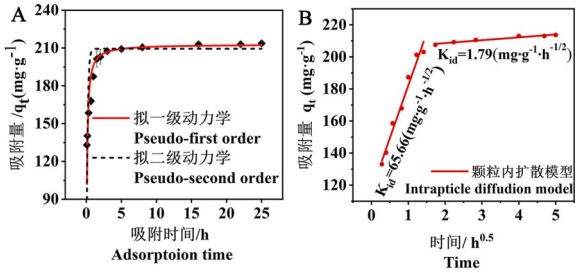

图4　修复剂吸附铅的动力学模型:拟一级动力学模型、拟二级动力学模型(A)和颗粒内扩散模型(B)

Fig.4　Kinetic model of lead adsorption by restorative: pseudo-first-order kinetic model, pseudo-second-order kinetic model (A) and intra-particle diffusion model (B)

表5　修复剂吸附铅的动力学参数

Table 5　Kinetic parameters of lead adsorption by restorative

样品 Sample	拟一级动力学模型 Pseudo-first order model			拟二级动力学模型 Pseudo-second order model		
	K_1/(h^{-1})	q_e/(mg·g^{-1})	R^2	K_2/(h^{-1})	q_e/(mg·g^{-1})	R^2
JK	3.879	178.19	0.936	7.350	181.83	0.977
JK−B	6.283	209.39	0.684	11.480	212.91	0.920

2.3.2　吸附热力学分析

在修复剂用量为0.4 g·L^{-1}、溶液初始pH=4、吸附时间为24 h的条件下,研究了溶液初始浓度和温度对铅吸附的影响。根据Langmuir和Freundlich等温线模型,对实验结果进一步拟合。其拟合曲线和参数分别见图5A和表7。从表中的相关系数R^2可知,Langmuir模型在不同的温度条件下对实验数据的拟合度均高于Freundlich模型($R^2_{1\ adj}>R^2_{2\ adj}$),说明修复剂具有均匀的表面和吸附位点,且铅以单分子层形式吸附于修复剂表面[30]。根据Langmuir吸附常数按照公式计算出平衡参数R_L,在不同浓度下(100~600 mg·L^{-1})的R_L值均为0~1,表明在不同温度条件,该修复剂对铅的吸附都是有利的。由Langmuir模型计算出其最大吸附能力为228.50 mg·g^{-1},与之前报道的铅吸附材料相比处于较高的水平,表明所制备的修复剂对铅具有优异的吸附性能[2,28,31]。

表6　修复剂吸附铅的颗粒扩散模型参数

Table 6　Parameters of particle diffusion model for lead adsorption by restorative

样品 Sample		颗粒内扩散模型 Weber−Morris intraparticle diffusion model		
		K_3/(mg·g^{-1}·h$^{-1/2}$)	C/(mg·g^{-1})	R^2
JK−B	Ⅰ	65.655	116.590	0.975
	Ⅱ	1.787	205.051	0.949

热力学研究结果及相关参数如图5B和表8所示。在不同的温度条件下均有$\Delta G<0$,表明吸附反应可以自发进行,随着温度的升高$|\Delta G|$增大,反应的自发性与温度呈正相关[28];$\Delta H>0$,进一步说明该修复剂对铅吸附过程是吸热的,升温有利于反应的进行[32];$\Delta S>0$说明反应朝熵增方向进行[33],这是因为修复剂吸附铅时,铅从本体溶液向外转移,导致熵增加[34]。综上所述,热力学分析结果表明,修复剂对铅的吸附是高温下的自发反应,温度升高促进反应的发生。

2.3.3　官能团分析

图6A为吸附铅前后的傅里叶变换红外光谱图。吸附反应前913 cm^{-1}和1389 cm^{-1}左右出峰,说

表7　修复剂吸附铅的等温吸附模型参数

Table 7　Isothermal adsorption model constants of lead on restorative

样品 Sample	T/K	朗缪尔吸附模型 Langmuir model			弗洛因得利克模型 Freundlich model			R_L
		q_m/(mg·g^{-1})	K_L/(L·mg^{-1})	R_1^2	K_F/(mg·g^{-1}(L·mg^{-1})$^{1/n}$)	n	R_2^2	
JK−B	288	204.19	0.043 42	0.991	110.256	10.978	0.952 0	$0<R_L<1$
	298	216.32	0.039 20	0.996	114.275	10.312	0.960 0	$0<R_L<1$
	309	228.50	0.036 63	0.984	112.278	9.297	0.964 9	$0<R_L<1$

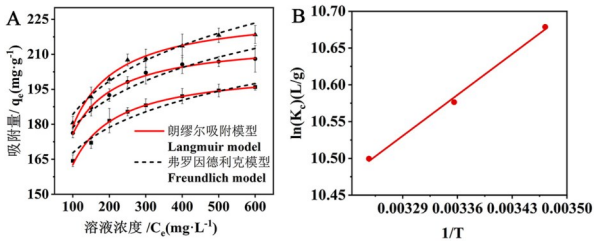

图5 修复剂对铅的等温吸附模型与吸附热力学分析:Langmuir和Freundlich模型拟合(A);温度对平衡常数的影响(B)

Fig.5 Isothermal adsorption model and adsorption thermodynamics analysis of lead by restorative: Langmuir and Freundlich model fitting (A); Effect of temperature on equilibrium constant (B)

表8 修复剂吸附铅的热力学参数

Table 8 Thermodynamic parameters of lead adsorption in restorative

样品 Sample	温度 T	ΔG/(KJ·mol^{-1})	ΔH/(KJ·mol^{-1})	ΔS/(KJ·mol^{-1}·K^{-1})
JK−B	288	−25.569	6.920	0.066
	298	−26.203		
	309	−26.886		

明羧酸结构C=O的存在[35]。吸附铅后,3296 cm^{-1}出现较宽的-OH伸缩振动,并且913 cm^{-1}左右C=O的半峰宽缩小且红移,1389 cm^{-1}处的峰消失,说明羟基、羰基等阴离子活性位点可能参与了铅的吸附[5]。N-H和C-N之间能耦合成酰胺Ⅱ带,一般吸收峰出现在1520~1570 cm^{-1}。位于1560 cm^{-1}处的峰为酰胺的Ⅱ带N-H键的弯曲和C-N的拉伸,吸附铅后,该峰移动至1546 cm^{-1},推测铅与酰胺基发生反应[36]。红外分析表明,羟基、羧基、羰基、酰胺基等官能团参与了铅的吸附。

图6B吸附铅前后的X射线衍射谱图。吸附前修复剂表面仅有C1s、N1s、O1s和Si2p等元素特征峰,吸附后新增Pb4f的特征峰,表明铅成功吸附于修复剂上。修复剂的O1s谱图如6C所示,吸附后O1s结合能从531.36 eV转移到531.26 eV,说明O^{2-}参与了吸附过程。O1s可分为C=O、C-OH和O-Metal共3个峰,吸附后,C-OH的相对含量从25.62%下降至23.56%,C=O的相对含量从52.19%下降至29.31%,而O-Metal的含量从22.19%上升至39.81%,结果表明吸附后修复剂表面存在铅与-COOH的化学键。此外,从图6D中可以看出,吸附后的N1s结合能从399.29 eV转移到399.02 eV,表明N元素参与了铅的吸附过程。修复剂的N1s光谱可分为两个峰,其化学形态主要为-NH和C=N[1],吸附铅之后,-NH的相对含量从65.62%上升至89.19%,C=N的相对含量从34.38%下降至16.81%,且有明显的位移。这是铅吸附过程成中N原子的电子云密度变化所致[37],可能的吸附机制是铅与酰胺基之间形成配位键,与傅里叶变换红外光谱的分析结果一致。

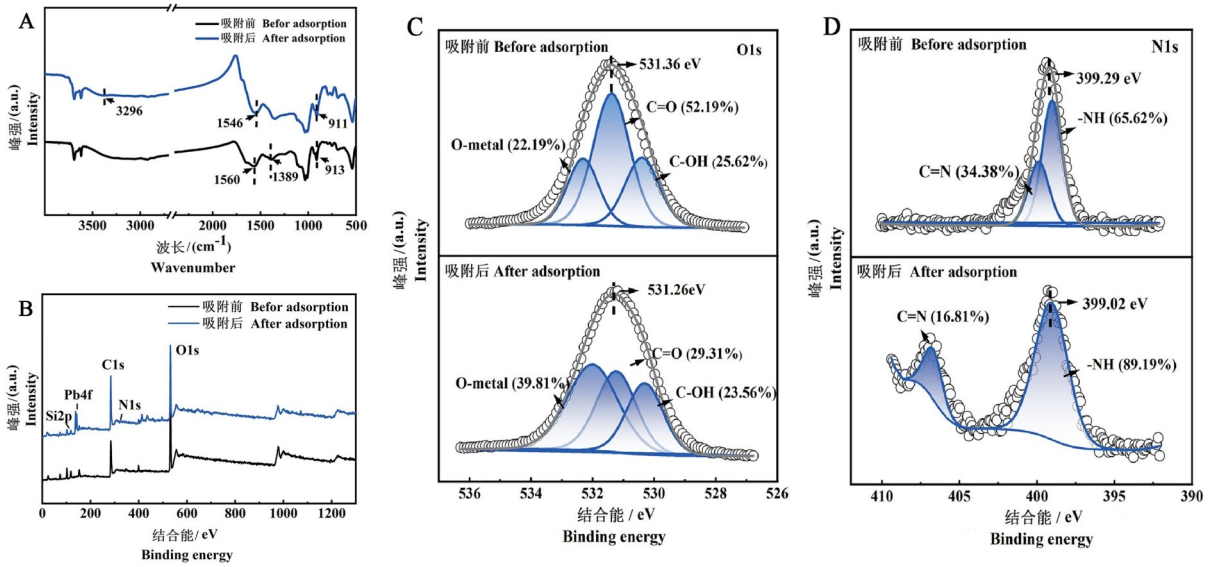

图6 吸附前后的傅里叶变换红外光谱图(A)、X射线衍射谱图(B)、O1s分谱(C)和N1s分谱(D)

Fig.6 FTIR (A), XPS (B), O1s (C) and N1s (D) spectra before and after adsorption

综上所述,该吸附过程以化学吸附为主,物理吸附为辅[38]。其主要吸附机制如下(图7):(1)铅首先从本体溶液转移到固液界面,然后通过物理吸附和静电引力被分散至修复剂周围;(2)修复剂表面的-OH、-COOH、C=O、和CO-NH_2等活性基团通过络合或配位作用快速的捕获铅;(3)此外,改性过程中形成的复杂微孔结构也是其吸附性能提高的重要原因。

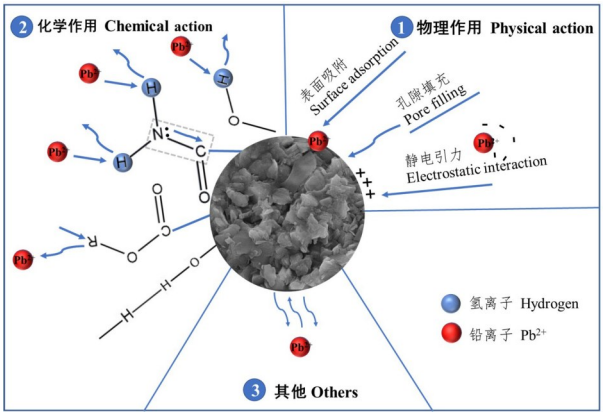

图7　吸附机制示意图

Fig.7　Schematic diagram of adsorption mechanism

3　结论

经过乙烯胺改性及相应曲面工艺优化,获得了一种风化煤改性修复剂JK-B,其改性工艺为:体系pH=4.98、乙烯胺用量2.58 mL·5g^{-1}风化煤、超声时间为64.34 min、超声功率为350 W;该修复剂对铅的吸附过程符合拟二级动力学模型和Langmuir模型,表明该过程是以化学吸附为主的单分子层吸附,最大吸附容量达228 mg·g^{-1},较原煤提高了48%;热力学分析显示ΔG<0、ΔH>0、ΔS>0,即该反应是高温下的自发反应,温度升高促进反应的发生;复杂的微孔结构以及羟基、羧基、羰基、酰胺基等活性基团是其吸附铅的主要机制。

参　考　文　献

[1]Tang J L, Chen Y B, Zhao M H, et al. Phenylthiosemicarbazide-functionalized UiO-66-NH_2 as highly efficient adsorbent for the selective removal of lead from aqueous solutions [J]. Journal of Hazardous Materials, 2021, 413: 125278.

[2]Tran H N, Nguyen D T, Le G T, et al. Adsorption mechanism of hexavalent chromium onto layered double hydroxides-based adsorbents: a systematic in-depth review [J]. Journal of Hazardous Materials, 2019,373: 258-270.

[3]Xu D M, Fu R B, Liu H Q, et al. Current knowledge from heavy metal pollution in Chinese smelter contaminated soils, health risk implications and associated remediation progress in recent decades: a critical review [J]. Journal of Cleaner Production, 2021,286: 124989.

[4]Jia X L, Fu T T, Hu B F, et al. Identification of the potential risk areas for soil heavy metal pollution based on the source-sink theory[J]. Journal of Hazardous Materials, 2020,393: 122424.

[5]Samimi M, Shahriari-Moghadam M. Isolation and identification of Delftia lacustris Strain-MS3 as a novel and efficient adsorbent for lead biosorption: kinetics and thermodynamic studies, optimization of operating variables[J]. Biochemical Engineering Journal, 2021,173: 108091.

[6]刘秀珍, 赵兴杰, 郭丽娜, 等. 膨润土和沸石对重金属镉的吸附性研究[J]. 山西农业大学学报(自然科学版), 2009,29(2): 97-99,103.
Liu X Z, Zhao X J, Guo L N, et al. Adsorption study of bentonite and zeolite on the heavy metal cadmium[J]. Journal of Shanxi Agricultural University (Natural Science Edition), 2009,29(2): 97-99,103.

[7]Mu X, Wang Z X, Liu L C, et al. Multiple exposure pathways of first-year university students to heavy metals in China: serum sampling and atmospheric modeling [J]. Science of the Total Environment, 2020,746:141405.

[8]Gao L, Li Z H, Yi W M, et al. Impacts of pyrolysis temperature on lead adsorption by cotton stalk-derived biochar and related mechanisms[J]. Journal of Environmental Chemical Engineering, 2021,9(4): 105602.

[9]张静静, 赵永芹, 王菲菲, 等. 膨润土、褐煤及其混合添加对铅污染土壤钝化修复效应研究[J]. 生态环境学报, 2019,28(2): 395-402.
Zhang J J, Zhao Y Q, Wang F F, et al. Immobilization and remediation of Pb contaminated soil treated with bentonite, lignite and their mixed addition[J]. Ecology and Environmental Sciences, 2019,28(2): 395-402.

[10]来雪慧, 王芳丽, 苗秀荣, 等. 小麦秸秆生物质炭与猪粪施用对小白菜镉吸收和生长的影响[J]. 山西农业大学学报(自然科学版), 2021,41(2):109-118.
Lai X H, Wang F L, Miao X R, et al. Effects of combined application of wheat straw biochar and pig manure on the growth rate of pakchoi and cadmium uptake ability from soil [J]. Journal of Shanxi Agricultural University (Natural Science Edition), 2021,41(2): 109-118.

[11]Meunier N, Drogui P, Montané C, et al. Comparison between electrocoagulation and chemical precipitation for metals removal from acidic soil leachate [J]. Journal of Hazardous Materials, 2006,137(1): 581-590.

[12]Sun Y B, Wu Z Y, Wang X X, et al. Macroscopic and microscopic investigation of U(VI) and Eu(III) adsorption on carbonaceous nanofibers [J]. Environmental Science & Technology, 2016,50(8): 4459-4467.

[13]Gao J, Sun S P, Zhu W P, et al. Chelating polymer modified P84 nanofiltration (NF) hollow fiber membranes for high efficient heavy metal removal[J]. Water Research, 2014, 63: 252-261.

[14]Vardhan K H, Kumar P S, Panda R C. A review on heavy metal pollution, toxicity and remedial measures: current trends and future perspectives [J]. Journal of Molecular Liquids, 2019,290: 111197.

[15]Liu L Q, Huang Y J, Meng Y H, et al. Investigating the adsorption behavior and quantitative contribution of Pb^{2+} adsorption mechanisms on biochars by different feedstocks from a fluidized bed pyrolysis system [J]. Environmental Research, 2020,187: 109609.

[16]Parmar P, Shukla A, Goswami D, et al. Optimization of cadmium and lead biosorption onto marine Vibrio alginolyticus PBR1 employing a Box-Behnken design [J]. Chemical Engineering Journal Advances, 2020,4: 100043.

[17]肖尧, 吴晨捷, 蒋庆肯, 等. 固定化Acinetobacter sp. T1细菌处理河道氨氮污染的研究[J]. 生态与农村环境学报, 2019, 35(10):1338-1345.
Xiao Y, Wu C J, Jiang Q K, et al. Study on the treatment of urban polluted water by immobilized *Acinetobacter* sp. T1 bacteria [J]. Journal of Ecology and Rural Environment, 2019, 35(10): 1338-1345.

[18]张杰, 朱晓丽, 尚小清, 等. 生物炭固定化解磷菌对Pb^{2+}的吸附特性[J]. 环境污染与防治, 2019,41(4):387-392.
Zhang J, Zhu X L, Shang X Q, et al. Adsorption characteristics of Pb^{2+} on biochar immobilized phosphate-solubilizing bacteria[J]. Environmental Pollution & Control, 2019,41(4): 387-392.

[19]陈诚, 郭俊元, 周明杰, 等. 壳聚糖—海藻酸钠固定化菌小球处理猪场沼液[J]. 中国环境科学, 2019,39(7):2812-2821.
Chen C, Guo J Y, Zhou M J, et al. Removal of ammonium from aqueous solution by microorganism cells immobilized into chitosan-sodium alginate beads [J]. China Environmental Science, 2019,39(7): 2812-2821.

[20]张可, 刘福义, 陈伟, 等. 玉米芯吸附-海藻酸钠固定微生物对十溴联苯醚的降解[J]. 应用与环境生物学报, 2016,22(5):904-910.
Zhang K, Liu F Y, Chen W, et al. Degradation of decabromodiphenyl ether by corncob-sodium alginate sodium alginate immobilized bacteria[J]. Chinese Journal of Applied and Environmental Biology, 2016,22(5): 904-910.

[21]李廷梅, 于鲁冀, 范铮. 微生物复合固定化颗粒特征分析及去除河水氨氮效果的研究[J]. 环境污染与防治, 2015,37(8):7-11.
Li T M, Yu L J, Fan Z. Characteristics analysis of composite immobilized microorganism and its ammonia nitrogen removal effect in river water [J]. Environmental Pollution & Control, 2015,37(8): 7-11.

[22]武海英. 乙烯胺改性风化煤吸附剂的制备及对含锌废水的处理研究[D]. 乌鲁木齐:新疆师范大学, 2018.
Wu H Y. Study on the effect of zinc containing wastewater removal and preparation of ethylamine modified weathered coal adsorbent[D].Urumqi: Xinjiang Normal University, 2018.

[23]雷娟, 易筱筠. 块状花生壳吸附重金属的机理研究[J]. 山西农业大学学报(自然科学版), 2015,35(5):514-518,554.
Lei J, Yi X Y. Mechanism studie on the heavy metal adsorption of blocky peanut shell [J]. Journal of Shanxi Agricultural University (Natural Science Edition), 2015, 35(5): 514-518,554.

[24]Gao J, Xu H, Li Q J, et al. Optimization of medium for one-step fermentation of inulin extract from Jerusalem artichoke tubers using Paenibacillus polymyxa ZJ-9 to produce R,R-2,3-butanediol[J]. Bioresource Technology, 2010,101(18): 7076-7082.

[25]李占君, 刘运伟, 王洪学, 等. 基于Plackett-Burman和Box-Behnken设计优化超声诱导防风种子发芽方法[J]. 森林工程, 2022,38(1):76-85.
Li Z J, Liu Y W, Wang H X, et al. Optimization of ultrasonic induced germination of *Saposhnikovia* divaricate seeds based on plackett-burman and box-behnken design [J]. Forest Engineering, 2022,38(1):76-85.

[26]马晓利, 武海英, 陈平. 三乙烯四胺改性风化煤对废水中Ni^{2+}吸附机制[J]. 环境科学研究, 2018,31(2):337-344.
Ma X L, Wu H Y, Chen P. Adsorption of Ni^{2+} in wastewater by triethylenete-tramine modified weathered coal[J]. Research of Environmental Sciences,2018,31(2):337-344.

[27]魏金枝, 陈芳妮, 孙晓君, 等. 氨基修饰磁性氧化石墨烯吸附离子型染料性能[J]. 中国环境科学, 2016,36(7):2020-2026.
Wei J Z, Chen F N, Sun X J, et al. Adsorption performance of amino functionalized magnetic graphene oxide composite to ionic dyes[J]. China Environmental Science, 2016, 36(7): 2020-2026.

[28]Zhao F, Su C H, Yang W X, et al. In-situ growth of UiO-66-NH_2 onto polyacrylamide-grafted nonwoven fabric for highly efficient Pb(II) removal[J]. Applied Surface Science, 2020, 527: 146862.

[29]Ding W C, Dong X L, Ime I M, et al. Pyrolytic temperatures impact lead sorption mechanisms by bagasse biochars [J]. Chemosphere, 2014,105:68-74.

[30]Luo S L, Xu X L, Zhou G Y, et al. Amino siloxane oligomer-linked graphene oxide as an efficient adsorbent for removal of Pb(II) from wastewater[J]. Journal of Hazardous Materials, 2014,274: 145-155.

[31]Ahmad Z, Gao B, Mosa A, et al. Removal of Cu(II), Cd(II) and Pb(II) ions from aqueous solutions by biochars derived from potassium-rich biomass [J]. Journal of Cleaner Production, 2018,180: 437-449.

[32]Ren C R, Ding X G, Fu H Q, et al. Core - shell superparamagnetic monodisperse nanospheres based on amino-functionalized $CoFe_2O_4$@SiO_2 for removal of heavy metals from aqueous solutions[J]. RSC Advances, 2017, 7(12): 6911-6921.

[33]Ghasemi M, Naushad M, Ghasemi N, et al. A novel agricultural waste based adsorbent for the removal of Pb(II)

from aqueous solution: kinetics, equilibrium and thermodynamic studies [J]. Journal of Industrial and Engineering Chemistry, 2014,20(2): 454-461.

[34]Chen B, Cao Y R, Zhao H N, et al. A novel Fe^{3+}-stabilized magnetic polydopamine composite for enhanced selective adsorption and separation of Methylene blue from complex wastewater[J]. Journal of Hazardous Materials, 2020, 392: 122263.

[35]Song M, Wei Y X, Cai S P, et al. Study on adsorption properties and mechanism of Pb^{2+} with different carbon based adsorbents[J]. Science of the Total Environment, 2018,618: 1416-1422.

[36]Bai J, Yang X H, Du R Y, et al. Biosorption mechanisms involved in immobilization of soil Pb by Bacillus subtilis DBM in a multi-metal-contaminated soil [J]. Journal of Environmental Sciences, 2014,26(10):2056-2064.

[37]Wu P, He Y Y, Lu S Y, et al. A regenerable ion-imprinted magnetic biocomposite for selective adsorption and detection of Pb^{2+} in aqueous solution[J]. Journal of Hazardous Materials, 2021,408:124410.

[38]Ifthikar J, Wang J, Wang Q L, et al. Highly efficient lead distribution by magnetic sewage sludge biochar: sorption mechanisms and bench applications [J]. Bioresource Technology, 2017,238:399-406.

Preparation and adsorption mechanism of modified weathered coal lead remediating agent

Jiao Zile[1,2], Li Lin[1,2], Chen Xiaojing[1,2,3], Lu Jinjing[1,2], Gao Chunhua[1,2], Xu Minggang[1,2], Li Jianhua[1,2*]

(*1.College of Resources and Environment, Shanxi Agricultural University, Taiyuan 030031, China; 2.Shanxi Province Key Laboratory of Soil Environment and Nutrient Resources, Taiyuan 030031, China; 3.Institute of Loess Plateau, Shanxi University, Taiyuan 030006, China*)

Abstract:[Objective]Weathered coal is widely available and inexpensive, and has the characteristics of reasonable pore size distribution and rich in active functional groups. Its adsorption performance can be improved through modification, and it can be used for treating high concentration heavy metal wastewater and thus is of great developmental value. The purpose of this paper was to prepare an efficient lead remediation agent with weathered coal as the raw material and to explore its adsorption mechanism, providing a material basis and theoretical support for the purification of lead-containing wastewater direction for the high-value utilization of weathered coal. [Method]Vinylamine modification and response surface methods were used to prepare and optimize the preparation process of weathered coal remediation agent. The adsorption mechanism of the material was investigated using batch adsorption experiments combined with characterization techniques such as Scanning Electron Microscopy (SEM), Specific Surface and Porosity Analyzer (BET), Fourier Transform Infrared Spectroscopy (FT-IR), X-ray Diffraction (XPS). [Result] The process parameters for preparing the lead remediation agent with triethylenetetramine-modified weathered were determined: System pH=4.98, ethylene amine dosage 2.58 $mL\cdot g^{-1}$ weathered coal, ultrasonic time 64.34 min, ultrasonic power 350 W. The adsorption process of the remediation agent on lead was in accordance with the pseudo-second-order kinetic model and Langmuir model, indicating that the process was predominantly monolayer adsorption through chemisorption, with a maximum adsorption capacity of 228 $mg\cdot g^{-1}$, which was a 48% increase over the raw coal. Thermodynamic analysis showed that $\Delta G<0$, $\Delta H>0$, $\Delta S>0$, indicating that the reaction was a spontaneous endothermic process, and the increase in temperature promoted the reaction. The disruption effect of ultrasonic modification and the grafting of polyethylene polyamines reduced the mesopore area by 63.14% and increased the micropore area by 126%, while the surface-rich hydroxyl, carboxyl, carbonyl, and amide groups coordinated or complexed with lead, facilitating its capture of lead. [Conclusion]This study obtained an efficient lead remediation material. The amount of ethylamine and ultrasonic temperature were the significant factors affecting the adsorption performance of the material. The increase in micropore area and the abundance of active groups (hydroxyl, carboxyl, carbonyl, amide) were the main lead adsorption mechanisms.

Keywords:Weathered coal, Vinylamine modification, Lead pollution, Response surface method

(编辑:马荣博)